Scenario of multiple filamentation and supercontinuum generation in a high-power femtosecond laser pulse

O.G. Kosareva, N.A. Panov, and V.P. Kandidov

International Laser Center of the Moscow State University, Moscow

The formation and development of multiple filaments along the propagation path of a high-power femtosecond laser pulse have been studied. By means of 3D+time numerical simulations, we have demonstrated the "birth," "competition," and "death" of filaments along the propagation path. The effect of the separation between inhomogeneities in the initial beam profile on the conversion efficiency of the input pulse energy into the supercontinuum energy has been investigated. The decrease in the separation between two inhomogeneities has been shown to be the cause of the increase in the conversion efficiency.

Introduction

The phenomenon of breakdown of a laser pulse field into filaments (from here on, *multifilamentation*) was discovered in liquids in the mid 1960s.[1] With the advent of high-power femtosecond lasers, it became possible to observe multiple filaments in gases, in particular, in the atmospheric air.[2,3] The investigation of multiple filaments in the atmosphere was addressed in Refs. 4 and 5. The fusion of two filaments upon the geometric focusing of a laser beam was studied in Ref. 4. The interference of conical emission rings from each of the filaments formed from two initial inhomogeneities at the transverse profile of the pulse intensity was observed in Ref. 5. In addition, in Ref. 5 the common properties of interference patterns from rings of multiple filaments were explained on the basis of a simple phenomenological model. The formation of multiple filaments at a large negative chirp of the initial pulse (0.5—9.5 ps with the duration of the spectrally limited pulse amounting to about 100 fs) was examined in Ref. 6.

Multifilamentation arises when the pulse power exceeds the critical self-focusing power by a sufficiently large value at almost any deviations of the transverse beam profile from the unimodal one. Such deviations are caused by fluctuations of the light field intensity distribution, which appear upon the intensification of the laser pulse,[7] and by the following increase in the amplitude of these fluctuations due to self-focusing in elements of the optical systems.[8] In addition, at the stage of filament formation, random distortions in the turbulent atmosphere are significant.[9] Therefore, multifilamentation almost inevitably arises upon the propagation of a high-power laser pulse in real media.

The filamentation of femtosecond pulses is usually accompanied by the generation of broadband radiation in the wavelength region from 400 to about 4500 nm [Ref. 10]. This effect, referred to as the *supercontinuum generation*, can be employed in a laser lidar for broadband sensing of the atmosphere.[11]

The spatial structure of the supercontinuum was studied experimentally in Refs. 8, 12—15. In Refs. 11 and 12, it was found that the supercontinuum radiation in the blue part of the spectrum is generated both at the filament axis and in the rings about the filament, while the supercontinuum radiation in the red part of the spectrum is generated only at the filament axis. The interference of the supercontinuum fields in the blue region in air was observed in Ref. 14 and investigated in detail in Ref. 8. In Ref. 15, the interference of the blue wing of the supercontinuum was discovered in the case of propagation of a femtosecond laser pulse in water.

Most of the theoretical studies of the filamentation and supercontinuum generation were performed in the approximation of the axisymmetric geometry,[16–18] which does not allow, in principle, the consideration of multifilamentation. In Refs. 19—21, the nonstationary multifilamentation was investigated in the coordinates x, y, z, t. One of the methods to control the multifilamentation was proposed in Ref. 20. In addition, the spatial distributions of the supercontinuum in the red and blue parts of the spectrum upon the multifilamentation have been analyzed theoretically in Ref. 8. At the same time, the mechanism of appearance of multiple filaments in a femtosecond laser pulse has not been studied.

In this paper, we study in detail the scenario of consecutive birth and death of filaments in a high-power laser pulse. It is shown that the efficiency of supercontinuum generation increases upon the decrease in the separation between the initial intensity perturbations in the beam profile.

Mathematical formulation of the problem

The propagation of a pulse through a medium is described by the equation for a slowly varying complex amplitude of the light field $E(x, y, z, t)$

©   2005   Institute   of   Atmospheric   Optics

$$2ik\left(\frac{\partial}{\partial z} + \frac{1}{v_g}\frac{\partial}{\partial t}\right)E = \frac{\partial^2 E}{\partial x^2} + \frac{\partial^2 E}{\partial y^2} + \frac{2k^2}{n_0}\Delta n E, \quad (1)$$

where v_g is the group velocity; $k = 2\pi/\lambda$ is the wave number; n_0 is the refractive index of the medium; the nonlinear addition to the refractive index Δn is defined as

$$\Delta n = \Delta n_{kerr} - \frac{2\pi e^2 N_e}{m(\omega^2 + \nu_c^2)}\left(1 + i\frac{\nu_c}{\omega}\right), \quad (2)$$

where Δn_{kerr} is the nonlinear addition to the refractive index associated with the Kerr nonlinearity; m and e are the electron mass and charge, respectively; ω is the frequency of laser radiation corresponding to the wavelength $\lambda = 810$ nm; $\nu_c = N_a v_e \sigma_c$ is the frequency of electron collisions with neutral particles [22]; N_a is the concentration of neutral particles (molecules or atoms); v_e is the root-mean-square velocity of electrons, acquired under the effect of the field E; σ_c is the collision cross section; N_e is the electron number density. The first term in Eq. (2) describes the instantaneous Kerr nonlinearity, while the second term describes the nonlinearity of the self-induced laser plasma.

The equation for the electron number density $N_e(x, y, z, t)$:

$$\frac{\partial N_e}{\partial t} = P(|E|^2)(N_a - N_e) + \nu_i N_e - \beta N_e^2. \quad (3)$$

is solved together with Eq. (1). The first term in the right-hand side of Eq. (3) describes the increase in the concentration of free electrons due to multiphoton ionization. The probability of multiphoton ionization $P(|E|^2)$ is determined according to Ref. 23. The second term in the right-hand side of Eq. (3) describes the avalanche increase in the number of free electrons. Here ν_i is the frequency of avalanche ionization, which is determined, according to Ref. 22, as follows:

$$\nu_i = \frac{1}{W_g}\frac{e^2 E^2}{2m(\omega^2 + \nu_c^2)}\nu_c, \quad (4)$$

where W_g is the ionization potential of air molecules (nitrogen and oxygen) or the width of the forbidden zone for water. The electron–ion recombination is described by the third term in the right-hand side of Eq. (3). The coefficient β (cm³/s) was determined, according to Ref. 24, as:

$$\beta = \frac{8.75 \cdot 10^{-27}}{T^{9/2}}N_e, \quad (5)$$

where T is the electron temperature in plasma, in eV.

Thus, the model (1)–(5) describes the diffraction of a laser pulse, its Kerr self-focusing, defocusing in the self-induced laser plasma, arising due to the multiphoton ionization and electron avalanche, the energy loss for ionization of the

medium, and the absorption in plasma. In the model proposed, we neglect the change in the shape of the ultrashort pulse as a result of the material dispersion and the lag effect of the Kerr nonlinearity.

Since this paper focuses on the influence of the non-unimodal spatial profile of the input beam on the multifilamentation of radiation, the change in the shape of the ultrashort pulse due to the material dispersion in the medium is ignored. In Ref. 16, it was shown that the material dispersion influences the shape of the pulse and the efficiency of conversion of the initial pulse energy into the supercontinuum, whereas the spatial distribution of the radiation energy density varies only slightly. Actually, the filament diameter in air amounts to 50−100 µm, that is, the length of its diffraction spreading for the radiation at the wavelength of 810 nm is no longer than ~ 2 cm. At the same time, the characteristic time scale, arising in the process of radiation self-focusing, is ~ 10 fs. The length of dispersion spreading, corresponding to this time scale, is ~ 1 m. Thus, the spatial effects determining the picture of multifilamentation develop faster than the temporal ones. In water, the filament diameter is about 10 µm (Ref. 25) and the length of diffraction spreading decreases to 200 µm. For the time scale of 10 fs, the length of dispersion spreading in water is 1000 µm, that is, in condensed media the spatial effects develop faster than the temporal ones too.

The nonlinear addition to the refractive index, associated with the Kerr nonlinearity, can be written in the form

$$\Delta n_{kerr} = \frac{1}{2}n_2\left\{(1 - \tilde{n})|E(t)|^2 + \tilde{n}\int_{-\infty}^{t}H(t - t')|E(t')|^2 \, dt'\right\}, \quad (6)$$

where

$$H(t) = \text{step}(t)\Omega^2 \exp\left(-\frac{\Gamma t}{2}\right)\frac{\sin \Lambda t}{\Lambda}$$

is the response function; for air $\Lambda^2 = \Omega^2 - \frac{\Gamma^2}{4}$, $\Omega = 20.6$ THz, $\Gamma = 26$ THz; n_2 is the coefficient of Kerr nonlinearity of the medium; the coefficient $\tilde{n} = 1/2$ characterizes the ratio between the instantaneous and inertial contributions to Δn_{kerr} (Refs. 26 and 27). The characteristic response time of the non-instantaneous term in Eq. (6) is ~ 76 fs. Since the duration of the pulse, for which the numerical simulation is carried out, does not exceed 45 fs, the contribution from the instantaneous part can be taken into account efficiently, by integrating Eq. (6) for the Gaussian time distribution of radiation. As a result, the nonlinear addition (6) can be presented in the instantaneous form[5]:

$$\Delta n_{kerr}(t) = \frac{1}{2}n_{2eff}(t)|E(t)|^2,$$

where $n_{2eff}(t) \approx 0.6 n_2$ for the pulse duration of 45 fs. In our calculations, n_2 was taken equal to 10^{-19} cm²/W,

and the corresponding critical self-focusing power for the short pulse with the duration of 45 fs was $P_{cr} = 10$ GW.

In water, the contribution of the Kerr nonlinearity $\Delta n_{kerr}(t)$ was calculated as instantaneous,[25] and it was assumed that $n_{2eff} = n_2 = 2 \cdot 10^{-16}$ cm^2/W. The corresponding critical self-focusing power is $P_{cr} = 4$ MW.

During the filamentation of a high-power femtosecond pulse at the wavelength of 810 nm in atmospheric air, the peak intensity is $5 \cdot 10^{13}$– 10^{14} W/cm^2, and the maximum concentration of free electrons does not exceed 10^{17} cm^{-3} (at the concentration of the air constituent molecules $N_a = 2.7 \cdot 10^{19}$ cm^{-3}). The frequency of electron collisions with neutral particles ν_c is $\sim 2 \cdot 10^{12}$ s^{-1}. The time between collisions ~ 500 fs exceeds the pulse duration used in experiments on filamentation and in numerical simulation considered in this paper. The avalanche ionization in air does not occur for the time of pulse propagation. The recombination time ~ 1 ns, calculated for the electron concentration of 10^{17} cm^{-3} and the plasma temperature of 5 eV is much longer than the pulse duration. The rate equation (3) in the case of atmospheric air takes the form

$$\frac{\partial N_e}{\partial t} = P(|E|^2)(N_a - N_e).$$

The nonlinear addition to the refractive index (2) can be written as

$$\Delta n = \Delta n_{2eff}|E|^2 - 2\pi e^2 N_e /(m\omega^2).$$

In water, the concentration of neutral particles $N_a = 3.3 \cdot 10^{22}$ cm^{-3} exceeds the concentration of air molecules by more than 1000 times. At the radiation intensity of 10^{13} W/cm^2, the ionization frequency is $\nu_i \sim 2 \cdot 10^{14}$ s^{-1} and the time $1/\nu_i = 5$ fs is shorter than the pulse duration. Thus, the concentration of free electrons increases due to both the multiphoton and avalanche ionization. At the intensity of 10^{13} W/cm^2, the frequency of collisions in water $\nu_c \sim 2 \cdot 10^{15}$ s^{-1} is comparable with the radiation frequency $\omega = 2.3 \cdot 10^{15}$ s^{-1}. The nonlinear addition to the refractive index Δn and the equation for the plasma density are considered in the form (2) and (3), respectively.

The numerical simulation involved the calculation of the following distributions with a certain interval Δz:

energy density

$$J(x,y,z) = \int\limits_{-\infty}^{+\infty} I(x,y,z,\tau)d\tau,$$

intensity profiles

$$I(x = 0, y, \tau),$$

spectral intensity profiles $S(x, y, \omega)$, which were determined using the Fourier transform:

$$S(x,y,z,\omega) = \left| \int\limits_{-\infty}^{+\infty} E(x,y,z,\tau)e^{i\omega\tau}d\tau \right|^2, \qquad (7)$$

where $\tau = t - z/v_g$ is the current time.

Scenario of multifilamentation of a femtosecond laser pulse

As laser pulses with the peak power exceeding the critical self-focusing power several times propagate, several filaments can be formed, and the interaction between these filaments is significantly nonstationary. In the numerical simulation of this phenomenon, the distribution of the complex amplitude of the field at the entrance to water (at $z = 0$) is taken as a sum of two Gaussian functions:

$$E(x,y,0,\tau) = e^{-\tau^2/2\tau_0^2}\left\{ E_1 \exp\left[-\frac{x^2 + (y - y_0)^2}{2a_1^2} \right] + \right.$$

$$\left. + E_2 \exp\left[-\frac{x^2 + (y + y_0)^2}{2a_2^2} \right] \right\}, \qquad (8)$$

where $\tau_0 = 27$ fs is the pulse duration at the e^{-1} level; $y_0 = 0.22$ mm; beam radii are $a_1 \equiv a_0 = 0.22$ mm, $a_2 = 0.055$ mm; $E_1 = \sqrt{8\pi I_1/c}$, $I_1 = 2.25 \cdot 10^{12}$ W/cm^2, $E_2 = \sqrt{8\pi I_2/c}$, $I_2 = 8.1 \cdot 10^{11}$ W/cm^2. The diffraction perturbation length of the radius a_0 is $l_d = ka_0^2 = 37.5$ cm. The peak power of the pulse roughly fourfold exceeds the critical self-focusing power of the Gaussian pulse. At $z = 0$, the partial power of an inhomogeneity with the radius a_1 is 58% of the total power and that of an inhomogeneity with the radius a_2 is 42% of the total power. At $\tau = -\infty$, the initial concentration of free electrons is $N_e(x, y, z, \tau = -\infty) = 10^{10}$ cm^{-3} (Ref. 28).

To study the nonstationary formation of filaments, consider the evolution of the spatial distribution of the energy density $J(x, y)$ along the axis z, because it is just this characteristics that is used almost always in the experiments with pulses of femtosecond duration (Fig. 1).

At a distance $0 < z < 0.2l_d$, the intensity of inhomogeneities increases. Filaments are formed almost independently, as in the case of the pulse propagation in the single-filament mode. At this ratio between the partial powers of the initial inhomogeneities, two filaments turn out to be formed at roughly the same distance $z \approx 0.2l_d$ (Fig. 1b). Here the distance of formation of the developed filament is understood as such a distance along the axis z, at which the peak intensity of an inhomogeneity achieves the threshold ionization intensity (for water $I \sim 10^{13}$ W/cm^2). At the energy density distribution, rings are formed at $z \geq 0.2l_d$ due to defocusing in the plasma, induced by each of the filaments (see local minima in the region of the maximum energy density in Fig. 1b).
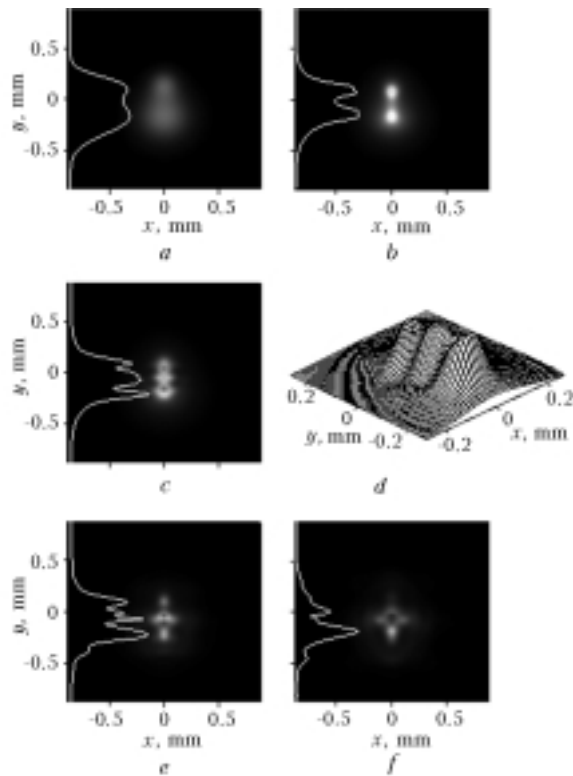
Fig. 1. Transverse distributions of the energy density at different distances z: ($z = 0$) initial conditions (*a*); ($z = 0.2l_d$) independent development of two filaments (*b*); ($z = 0.3l_d$) birth of a "daughter" filament as a result of interaction of ring structures of the "parent" filaments (*c*, *d*); ($z = 0.45l_d$) beginning of breakup of the upper filament (*e*); ($z = 0.55l_d$) "death" of the upper filament (*f*).

The ring structures of the formed "parent" filaments interfere, and at $z = 0.3l_d$ a developed "daughter" filament with the coordinates ($x = 0$, $y = -0.22a_0$) is formed, as one can see from Fig. 1*c*. Figure 1*d* shows the "birth" of the third filament in the form of a surface.

At $z \geq 0.4l_d$, the centroid of the distribution $J(x, y)$ begins to shift toward negative values of y, that is, the inhomogeneity with the high partial power begins to dominate. This is connected with the fact that at the distance $z = 0.45l_d$ the pulse looses about 30% of its initial energy, mostly because of the absorption in plasma. The filaments "struggle" for energy. As a result of this competition (Fig. 1*e*), one of the parent filaments disappear, and at $z = 0.55l_d$ high-intensity maxima remain only in the region $y < 0$ (Fig. 1*f*), that is, only one filament with the coordinates ($x = 0$, $y = -0.42a_0$), formed in the region of the initial perturbation with the higher partial power, survives in the competition.

To study the processes of independent development of the "parent" filaments, the interference of the ring structures from these filaments, and the formation of the daughter filament in a more detail, consider Fig. 2.

As can be seen from Fig. 2, the conical emission rings are formed at the distance $z \approx 0.2l_d$ and grow

quickly, achieving the diameters $d(z = 0.23l_d)|_{a_1} \approx$ $\approx 0.5a_0$ and $d(z = 0.23l_d)|_{a_2} \approx 0.4a_0$ by the distance $z = 0.23l_d$. At this distance, the stage of independent development of the parent filaments terminates, the ring structures approach each other to the minimum separation $\sim 0.3a_0$, and their interference begins. In the plot $d(z)$, this corresponds to the termination of the ring growth. During the further propagation to the distance $z \approx 0.26l_d$, the constructive interference of the ring structures from the parent filaments results in formation of the developed daughter filament with its own conical emission ring, and it is no longer possible to speak about the rings of the parent filaments.

The numerical simulation allows us to draw the time-resolved intensity distributions $I(x = 0, y, \tau)$, which carry voluminous information about the interaction of the filaments (Fig. 3). Figure 3*a* depicts the initial distribution $I(x = 0, y, z = 0, \tau)$ at the entrance to the nonlinear medium. Figure 3*b* and the corresponding Fig. 1*b* show the stages of independent development of the two parent filaments from the initial perturbations, and both of the filaments are already developed, because they have already formed the ring structures.
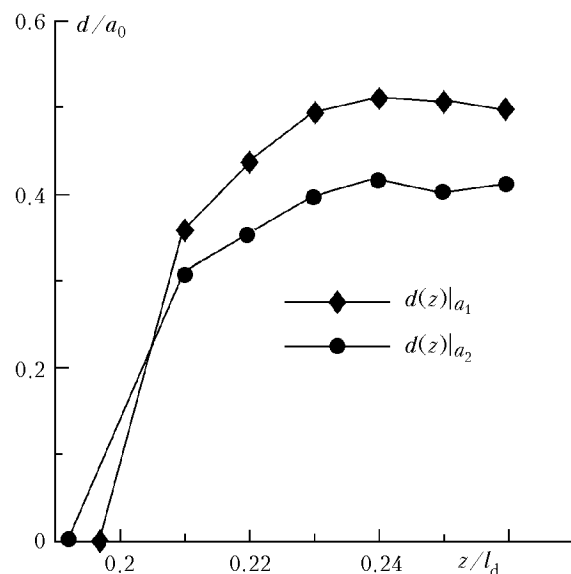

Fig. 2. Diameters d of the rings of the parent filaments as functions of the propagation coordinate z. The perturbation of the radius a_1 is shown by squares, and that of the radius a_2 is shown by circles.

By the distance $z = 0.3l_d$ (Fig. 3*c*), the third, daughter, filament is formed due to the interference of the conical emission rings from the parent filaments. It is important to note that the filaments appear in different time layers, for example, the daughter filament forms at the time layer $\tau = 0.9$ fs, while the parent filaments are formed at the layers $\tau = -14.5$ fs, located in the upper hemisphere, and $\tau = -16.9$ fs, located in the lower hemisphere.
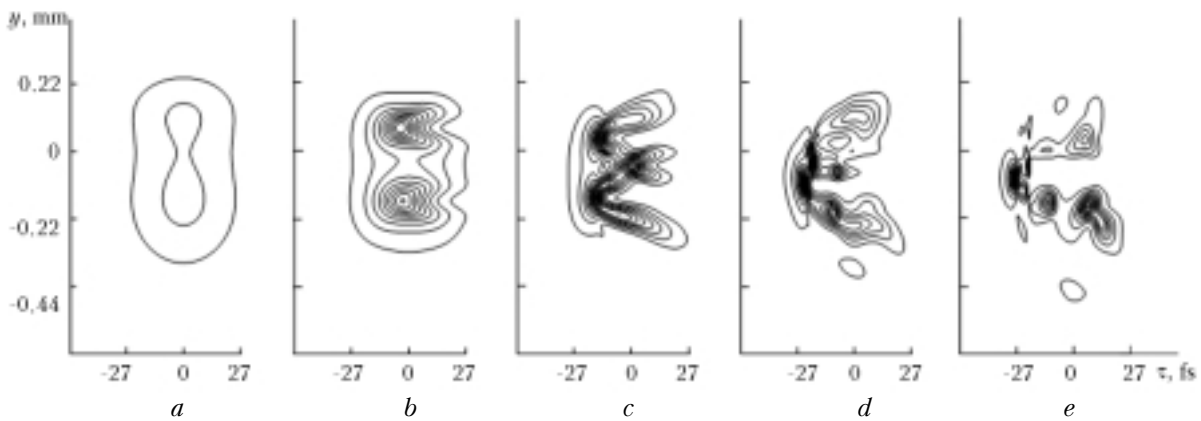
Fig. 3. Lines of equal intensity $I(x = 0, y, \tau)$ at the distance z: $(z = 0)$ initial conditions (a); $(z = 0.2l_d)$ independent development of two filaments (b); $(z = 0.3l_d)$ birth of the daughter filament as a result of interaction between ring structures of the parent filaments (c); $(z = 0.45l_d)$ beginning of breakup of the upper filament (d); $(z = 0.55l_d)$ death of the upper filament (e). The minimum level is $0.04I_{max}$, the step between the lines is $0.04I_{max}$ (I_{max} is the peak intensity at $z = 0.55l_d$).

In the process of laser pulse propagation, the pulse energy decreases due to dissipation in plasma and ionization of water molecules. At the distance $z > 0.45l_d$ (Fig. 3d), the filaments compete with each other, so that by $z = 0.55l_d$ only one filament, located in the lower hemisphere, survives (Fig. 3e).

Thus, we can separate the following stages of the interaction between multiple filaments during the propagation of the high-power femtosecond laser pulse:

— independent development of the initial perturbations in the spatial profile of the beam into the developed parent filaments;

— interference of the intensity rings, which spread in the cross section from the initially formed parent filaments,

— appearance of daughter filaments as a result of this interference;

— competition between the filaments, manifesting itself in the energy transfer from one filament to another;

— survival of one (or several) filament in the competition.

Generation of supercontinuum of multiple filaments

The blue supercontinuum radiation is generated both on the filament axes and in the rings spreading from each filament. In the case of multifilamentation, the interference between these rings is possible.[8] In the red part of the spectrum, the supercontinuum generation was detected only on the filament axes.[12,13]

To study the spatial distribution of the supercontinuum in air, the initial conditions at the entrance to the nonlinear medium (air) were taken in the form (8), where $E_1 = \sqrt{8\pi I_1/c}$, $I_1 = 1.93 \times \times 10^{13} \, \text{W/cm}^2$, $E_2 = \sqrt{8\pi I_2/c}$, $I_2 = 6.93 \cdot 10^{12} \, \text{W/cm}^2$, pulse energy $W_0 = 5 \, \text{mJ}$, beam radii $a_1 \equiv a_0 =$ = 0.18 mm, $a_2 = 0.045$ mm, the length, used for normalization of the propagation coordinate z, $l_d = ka_0^2 = 25.1$ cm. The peak power of the pulse is roughly 11 times exceeds the critical self-focusing power of the Gaussian beam. In the case of the close location of the initial perturbations on the transverse profile of the beam, y_0 was taken equal to $0.75a_0$. The upper row in Fig. 4 shows the successive formation of multiple filaments from two initial inhomogeneities. Note that all the main stages of the multifilamentation scenario are observed in air.

Two filaments develop independently of the initial perturbations, and by the distance $z = 0.08l_d$ the first parent filament, formed from the initial perturbation located in the upper half-plane, generate conical emission rings. First daughter filaments are formed from these rings (Fig. 4a). After the generation of the rings spreading from the filament located in the lower half-plane, a complex pattern of interference between the fields of multiple filaments (both parent, and daughter) arises, which results in the birth of new filaments (Fig. 4b). By the distance $z = 0.13l_d$, about eight filaments are formed (Fig. 4c).

When studying the spatial distributions of the supercontinuum at some distances z, the spectral intensity $S(x, y, z, \lambda)$ was determined by Eq. (7). Consider the evolution of the spatial distribution of $S(x, y, z, \lambda = 650 \, \text{nm})$, that is, in the blue wing of the spectral region (see Fig. 4, central row). The distances of detection of the supercontinuum in the numerical experiment correspond to the distances of detection of the energy density (see Figs. 4a–c). As is shown in Fig. 4d, the generation of the supercontinuum begins on the filament axes as a result of the phase self-modulation under the conditions of the Kerr nonlinearity of the medium. Then in the process of defocusing in the self-induced laser plasma, the spectral components in the high-frequency region of the supercontinuum begin to appear in the rings surrounding the filaments

(Figs. $4d$ and e). The detailed explanation to the spreading of the high-frequency components in the form of the rings surrounding the filament is given in Ref. 16. Simultaneous development of several filaments leads to interference between the rings of high-frequency components from different filaments (see Figs. $4e$ and f). The presence of interference indicates that the broadband radiation generated by each of multiple filaments born in a single pulse is coherent.

In the red wing of the supercontinuum spectral region, it is mostly generated on the filament axes (see Fig. 4, lower row). To confirm this, Figs. $4g-i$ show not only the distributions $S(x, y, z, \lambda = 850$ nm), but also the plots of the energy density at $x = 0$: $J(x = 0, y, z)$ — solid white lines. As can be seen, any region of active generation of the red

wing of the supercontinuum is connected with the corresponding filament. At the same time, the maxima of the spectral components at the wavelength $\lambda = 850$ nm could form earlier along the axis z. Since it is known that the red components of the supercontinuum propagate along the filament axes,[16] it is possible to expect the detection of the maxima of these components, corresponding to the position of born (and, possibly, already dead or significantly displaced) filaments at any distances z shorter than the distance of detection. An example of such a maximum is the peak located at the point ($x = 0$, $y = -0.135$ mm) in Fig. $4g$. The filament, which has generated this maximum, was formed at the distance $z \approx 0.08l_{\mathrm{d}}$ at the same values ($x = 0$, $y = -0.135$ mm), which roughly corresponds to the perturbation maximum in the profile of the input beam.
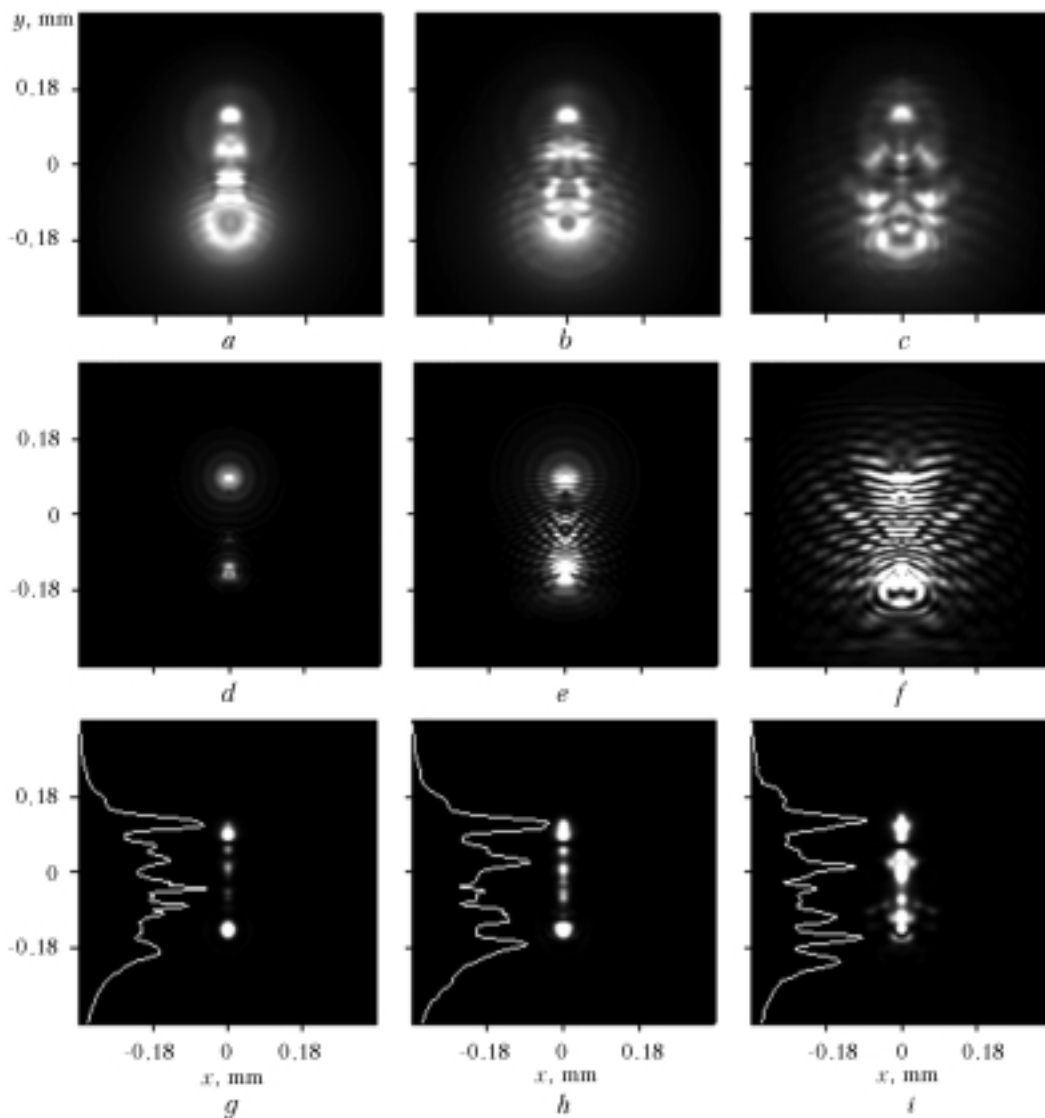

Fig. 4. Spatial distributions of the energy density $J(x, y, z)$ — upper row ($a-c$); spectral intensity of the supercontinuum $S(x, y, z, \lambda)$ in the blue region ($\lambda = 650$ nm) — central row ($d-f$), spectral intensity of the supercontinuum $S(x, y, z, \lambda)$ in the red region ($\lambda = 850$ nm) — lower row ($g-i$) at some distances z: $z = 0.10l_{\mathrm{d}}$ (a, d, g), $z = 0.11l_{\mathrm{d}}$ (b, e, h), $z = 0.13l_{\mathrm{d}}$ (c, f, i).

The spatial distribution of the spectral intensity obtained in the computer experiment is shown in Figs. $4d-i$ for the distance between perturbations $y_0 = y_{short} = 0.75a_0$. For the longer distance between perturbations $y_0 = y_{long} = 0.9a_0$, the area of interference between the conical emission rings in the blue region decreases. It is practically interesting to compare the efficiency of conversion of the laser pulse into the supercontinuum for the shorter and longer distances between initial perturbations. The supercontinuum energy in the blue W_{blue} and red W_{red} spectral regions is determined by the following equations:

$$W_{blue}(z) = \int_{\lambda_1}^{\lambda_2} S(x,y,z,\lambda)\mathrm{d}x\mathrm{d}y\mathrm{d}\lambda,$$

$$W_{red}(z) = \int_{\lambda_3}^{\lambda_4} S(x,y,z,\lambda)\mathrm{d}x\mathrm{d}y\mathrm{d}\lambda,$$

where $\lambda_1 = 400$, $\lambda_2 = 750$, $\lambda_3 = 850$, $\lambda_4 = 1000$ nm. The efficiency of conversion of the laser pulse energy into the supercontinuum is determined by the ratio of the energy of the blue (red) spectral portion to the total energy of the laser pulse at the entrance to the nonlinear medium W_0. Figure 5 shows the ratios W_{blue}/W_0 and W_{red}/W_0 as functions of the distance z.
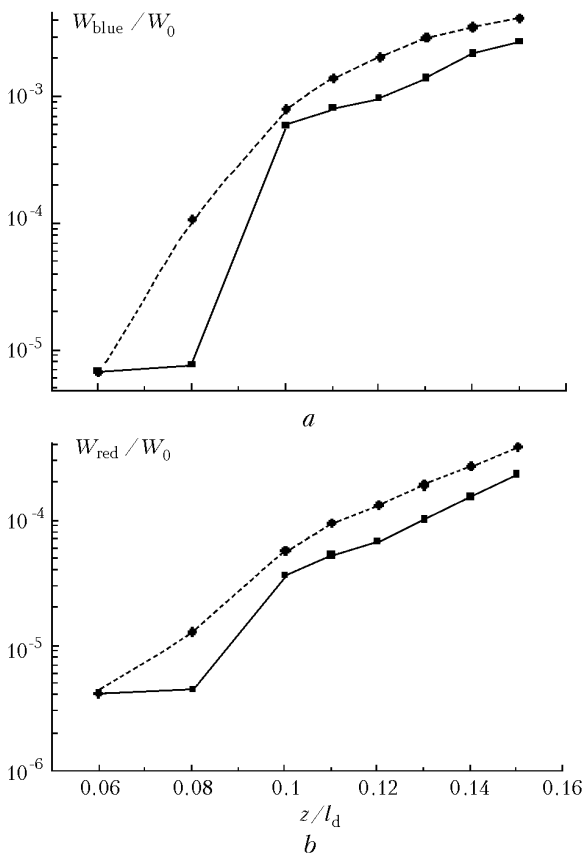

Fig. 5. Supercontinuum energy in the blue W_{blue} (*a*) and red W_{red} (*b*) spectral regions as a function of the distance z at the far (solid line) and close (dashed line) location of the initial perturbations; W_0 is the laser pulse energy at $z = 0$.

As can be seen from Fig. 5, the energy of the supercontinuum increases with the distance. In the blue spectral region at the distance $z = 0.10l_d$, the conversion efficiency achieves $8.0 \cdot 10^{-4}$ for close perturbations and $5.9 \cdot 10^{-4}$ for far perturbations. In the red spectral region, the efficiency of conversion into the supercontinuum is also higher in the case of close initial perturbations.

Thus, close location of the initial inhomogeneities is preferable for the transfer of the energy with the fundamental wavelength into the white light. This agrees with the experimental data on the influence of scaling of the beam dimensions on the signal of supercontinuum and nonlinear fluorescence.[29]

Conclusions

1. The scenario of formation of multiple filaments upon the propagation of a femtosecond laser pulse with the non-unimodal transverse intensity distribution includes:

− independent development of the initial perturbations in the spatial profile of the beam into the developed filaments, forming plasma "microchannels";

− interference between the rings in the intensity distribution, which spread in the cross section from the parent filament formed earlier;

− appearance of the daughter filaments caused by this interference;

− competition between the filaments that manifests itself in the energy transfer from one filament to another;

− survival of one (or several) filament as a result of the competition.

2. In the case of multifilamentation, the spatial distribution of the supercontinuum radiation in the red spectral region looks like a set of axisymmetric peaks with centers on the axes of the corresponding filaments. In the blue region, the interference is observed between the rings of the conical emission of the supercontinuum, spreading from each filament.

3. The decrease of the distance between the initial perturbations in the beam intensity profile leads to an increase in the efficiency of conversion of the laser pulse into the supercontinuum radiation.

Acknowledgments

References

1. R.Y. Chiao, M.A. Johnson, S. Krinsky, H.A. Smith, C.H. Townes, and E. Garmire, IEEE. J. Quant. Electron. **2**, No. 9, 467−469 (1966).

2. H. Schillinger and R. Sauerbrey, Appl. Phys. B **68**, No. 4, 753−756 (1999).

3. A. Braun, G. Korn, X. Liu, D. Du, J. Squier, and G. Mourou, Opt. Lett. **20**, No. 1, 73−75 (1995).

4. S. Tzortzakis,   L. Berge,   A. Couarion,   M. Franco, B. Prade, and A. Mysyrowicz, Phys. Rev. Lett. **86**, No. 24, 5470−5473 (2001).

5. S.L. Chin, S. Petit, W. Liu, A. Iwasaki, M.-C. Nadeu, V.P. Kandidov, O.G. Kosareva, and K.Yu. Andrianov, Opt. Commun. **210**, No. 9, 329−341 (2002).

6. G. Mechain, A. Couairon, Y.-B. Andre, C.D. Amico, M. Franco, B. Prade, S. Tzortzakis, A. Mysyrowicz, and R. Sauerbrey, Appl. Phys. B **79**, No. 3, 379−382 (2004).

7. S. Ito, H. Ishikawa, T. Miura, K. Takasago, A. Endo, and K. Torizuka, Appl. Phys. B **76**, No. 5, 497−503 (2003).

8. W. Liu, S.A. Hosseini, Q. Luo, B. Ferland, S.L. Chin, O.G. Kosareva, N.A. Panov, and V.P. Kandidov, New Journ. of Phys. **6**, No. 6, 6.1−6.22 (2004).

9. S.L. Chin,   A. Talebpour,   J. Yang,   S. Petit, V.P. Kandidov, O.G. Kosareva, and M.P. Tamarov, Appl. Phys. B **74**, No. 1, 67−76 (2002).

10. J. Kasparian,   R. Sauerbrey,   D. Mondelain, S. Niedermeier, J. Yu, J.-P. Wolf, Y.-B. Andre, M. Franco, B. Prade,   S. Tzortzakis,   A. Mysyrowicz,   M. Rodriguez, H. Wille, and L. Wöste, Opt. Lett. **25**, No. 18, 1397−1399 (2000).

11. J. Kasparian,   M. Rodrigues,   G. Mejean,   J. Yu, E. Salmon, H. Wille, R. Bourayou, S. Frey, Y.-B. Andre, A. Mysyrowicz, R. Souerbrey, J.-P. Wolf, and L. Wöste, Science **301**, No. 5629, 61−64 (2003).

12. E.T.J. Nibbering, P.F. Curley, G. Grillon, B.S. Prade, M.A. Franco, F. Salin, and A. Mysyrowicz, Opt. Lett. **21**, No. 1, 62−64 (1996).

13. O.G. Kosareva, V.P. Kandidov, A. Brodeur, C.Y. Chien, and S.L. Chin, Opt. Lett. **22**, No. 17, 1332−1334 (1997).

14. V.P. Kandidov, O.G. Kosareva, I.S. Golubtsov, W. Liu, A. Beckerc, N. Aközbek, C.M. Bowden, and S.L. Chin, Appl. Phys. B **77**, Nos. 2−3, 149−165 (2003).

15. K. Cook, A.K. Kar, and R.A. Lamb, Appl. Phys. Lett. **83**, No. 19, 3861−3863 (2003).

16. I.S. Golubtsov,   V.P. Kandidov,   and   O.G. Kosareva, Atmos. Oceanic Opt. **14**, No. 5, 303−315 (2001).

17. M. Kolesik,   G. Katona,   J.V. Moloney,   and E.M. Wright, Phys. Rev. Lett. **91**, No. 14, 043905−1−4 (2003).

18. N. Aközbek, M. Scalora, C.M. Bowden, and S.L. Chin, Opt. Commun. **191**, Nos. 3−6, 353−362 (2001).

19. M. Mlejnek,   M. Kolesik,   J.V. Moloney,   and E.M. Wright, Phys. Rev. Lett. **83**, No. 15, 2938−2941 (1999).

20. G. Mechain, A. Couairon, B. Prade, and A. Mysyrowicz, Phys. Rev. Lett. **93**, No. 3, 035003−1−4 (2004).

21. S.A. Hosseini, Q. Luo, B. Ferland, W. Liu, S.L. Chin, O.G. Kosareva,   N.A. Panov,   N. Aközbek,   and V.P. Kandidov, Phys. Rev. A (2004) (in press).

22. Yu.P. Raizer, *Gas Discharge Physics* (Nauka, Moscow, 1992), 536 pp.

23. A.M. Perelomov, V.S. Popov, and M.V. Terent'ev, Zh. Eksp. Teor. Fiz. **50**, No. 5, 1393−1410 (1966).

24. I.S. Golubtsov,   V.P. Kandidov,   and   O.G. Kosareva, Quant. Electron. **33**, No. 6, 525−530 (2003).

25. W. Liu, O.G. Kosareva, I.S. Golubtsov, A. Iwasaki, A. Becker, V.P. Kandidov, and S.L. Chin, Appl. Phys. B **76**, No. 3, 215−229 (2003).

26. M. Mlejnek, E.M. Wright, and J.V. Moloney, Opt. Lett. **23**, No. 5, 382−384 (1998).

27. E.T.J. Nibbering, G. Grillon, M.A. Franco, B.S. Prade, and A. Mysyrowicz, J. Opt. Soc. Am. B **14**, No. 3, 650 (1997).

28. Q. Feng, J.V. Moloney, A.C. Newell, E.M. Wright, K. Cook, P.K. Kennedy, D.X. Hammer, B.A. Rockwell, and C.R. Thompson, IEEE. J. Quant. Electron. **33**, No. 2, 127−137 (1997).

29. Q. Luo,   S.A. Hosseini,   W. Liu,   J.-F. Gravel, O.G. Kosareva, N.A. Panov, N. Aközbek, V.P. Kandidov, G. Roy, and S.L. Chin, Appl. Phys. B (2004) (in press).